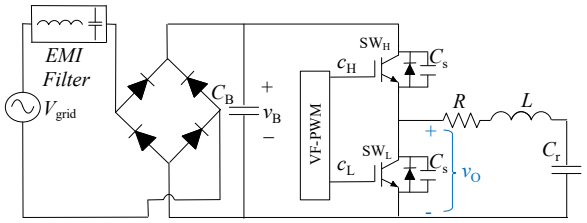

Fig. 1. Half-bridge series resonant inverter.

(for 50 Hz AC line) in v_B in order to increase the power factor and reduce cost [2]. The inverter generates a medium frequency (30 kHz - 70 kHz) ac-current that flows through the induction coil. The inductor-pan coupling is modeled as a series R-L circuit. The produced alternating magnetic field generates heat in the bottom of the metal cooking pan due to induced eddy currents losses. The complementary gate signals c_H and c_L are usually generated digitally with programmable dead time [3].

A variable frequency PWM can be digitally generated in several ways, as reported in the literature. It can be implemented using a counter and a comparator, as in on-chip timer peripherals available in microcontrollers and Digital Signal Processors (DSPs), or using a phase-accumulator and a comparator [4]. The latter has several advantages as pointed out in [4], and its hardware complexity is not bigger than that of the former. One advantage of the phase-accumulator based PWM (PAB-PWM) is that it operates in the frequency domain, i.e. the output frequency is proportional to its input parameter. However, the counter based PWM (CB-PWM) operates in the time domain since the frequency is set via period registers, i.e., the output frequency is inversely proportional to the input parameter. The PAB-PWM, unlike the CB-PWM, also features constant frequency resolution. Operating in the frequency domain is convenient when f_{sw} is the output variable of the controller that adjust the power delivered to the load [5], [6]; besides frequency and pulse width are set independently in the PAB-PWM; whereas the compare register must be changed accordingly to the period register in the CB-PWM in order to maintain D. Additionally, operating in the frequency domain is convenient when switching frequency modulation profiles are used as a spread spectrum technique to reduce conducted electromagnetic interferences in resonant inverters [7]. Furthermore, frequency and phase can be set independently what can be suitable when several PWM signals with the same frequency and duty cycle, that have constant phase relationships must be generated, such as in [8], [9].

Manuscript received March 23, 2018; revised May 6, 2018, July 14, 2018 and August 5, 2018; accepted September 2, 2018. This work was partly supported by the Spanish MINECO under Project TEC2016-78358-R and Project RTC-2017-5965-6, by the DGA-FSE, and by the BSH Home Appliances Group.

J. Villa, J. I. Artigas, J. R. Beltrán and L. A. Barragán are with the Department of Electronic Engineering and Communications, University of Zaragoza, Zaragoza, 50018 Spain (e-mail: jvillal@unizar.es; jiartigas@unizar.es; jrbelbla@unizar.es; barragan@unizar.es).

A. Domínguez is with the Department of Induction Technology of BSH Electrodomésticos, Bosch And Siemens Home Appliances Group, Zaragoza, 50016 Spain (e-mail: Alberto.Dominguez@bshg.com).

The PAB-PWM is an example of DDS (Direct Digital Synthesis) that has been used in digital signal processing to generate periodic waveforms, in particular, sine, triangle and square waves. It is also well-know that this scheme produces spurs when used to generate sine waves and jitter when used to generate square waves [10], [11]. When the PAB-PWM is used to operate an inverter in domestic IH applications, acoustic noise can be generated what may annoy the final users and concerns the manufacturers.

Acoustic noise has been extensively analyzed in the field of electric motors in the literature [12]–[17]. However, there are few articles on this subject in the field of domestic IH. Since, unlike in induction motors, the operating switching frequency is above the audible range in domestic IH systems [18]; acoustic noise is avoided operating the inverter at switching frequencies above 20 kHz using CB-PWM [1]. Assuming that the inverters use variable frequency control to adjust the power delivered to the load, audible noise can appear when two or more inverters connected to a common supply and sharing the same EMI filter are operated at the same time with different switching frequencies whose difference lies within the audible frequency range [19]. In order to avoid audible noise, some works [19]–[22] propose to operate the inverters with a switching frequency difference, in absolute value, smaller or equal than a given low frequency f_{L} or greater than another high frequency f_{H} according to a given threshold of audibility. The noise sources that exist in IH appliances are enumerated in [23]. In [24], a constraint in the PDM frequency is set to suppress audio noise from experimental results.

In this work, it is analyzed the audible noise in the range 5 kHz - 20 kHz that can be generated by one half-bridge series resonant inverter operated with PAB-PWM. We focus in this range because the boiling noise above 5 kHz is negligible [23] and tonal noise in this range is very annoying since it is a non-natural sound. The source of acoustic noise is electromagnetic due to Lorentz forces exerted on the pot bottom that can cause the pot to vibrate producing structure-borne acoustic noise. Since this force is proportional to the inductor current squared [25], the acoustic noise generation can be analyzed from the frequencies in the spectrum of i_{L}^2 that lie in the audible range. The relationship between the magnitudes will depend on the pot; and it is out of the scope of this work since it will require to solve a multi-physics problem involving electromagnetic, structural and acoustic phenomena [16]. Applying the windowing theorem [26], the harmonics of i_{L}^2 can be obtained from the harmonics of i_{L}.

The Spectral Flatness Measure (SFM) [27] will be used to quantify the noise-like or tone-like nature of the spectrum of i_{L}^2 in the band [5 kHz - 20 kHz]. For tonal signals, SFM is close to 0; and it is close to 1 for noise signals. Finally, two techniques [11], [28] that have been applied in the DDS literature to reduce spurs will be applied to the PAB-PWM modulator and their effect in the acoustic noise will be analyzed.

This paper is organized as follows. Section II determines the PAB-PWM design parameters for this application; calculates the tone frequencies that appear at the output of the PAB-PWM, presents the noise reduction techniques applied to PAB-PWM, and analyzes the current harmonic effect on magnetic force. Section III gives relevant simulation results. The experimental results obtained are summarized in Section IV. Finally, the main conclusions of this work are drawn in section V.

II. PAB-PWM Analysis

A conventional DDS has a phase accumulator and a phase to waveform converter. The phase accumulator PA has N bits; it accumulates the phase increment Δ every clock cycle and wraps around upon reaching the maximum value. Its output is a variable slope sawtooth wave that is converted to amplitude by a second block. In a PAB-PWM, the second block is a digital comparator that compares the accumulator with a reference value proportional to the duty cycle. The average switching frequency generated by the DDS is:

$$\langle f_{\mathrm{sw}} \rangle = \frac{\Delta}{2^N} f_{\mathrm{CLK}} \tag{1}$$

where f_{CLK} is the clock frequency. The smallest increment or decrement in the switching frequency $\Delta f_{\mathrm{sw,min}}$ is obtained by (1) with $\Delta = 1$. In a CB-PWM, the switching frequency generated is $f_{\mathrm{CLK}}/N_{\mathrm{C}}$, where N_{C} is the number of states of the free running counter. In this case, the smallest frequency increment or decrement is:

$$\Delta f_{\mathrm{sw}} = \frac{f_{\mathrm{CLK}}}{N_{\mathrm{C}}} - \frac{f_{\mathrm{CLK}}}{N_{\mathrm{C}}+1} \approx \frac{f_{\mathrm{sw}}^2}{f_{\mathrm{CLK}}}. \tag{2}$$

A. Design parameters

The average output power P delivered to the load considering only the fundamental harmonic and duty cycle $D = 0.5$ is [29]:

$$P \approx \frac{P_{\max}}{1 + Q^2 \left(\frac{f_{\mathrm{sw}}}{f_{\mathrm{o}}} - \frac{f_{\mathrm{o}}}{f_{\mathrm{sw}}} \right)^2} \tag{3}$$

where $P_{\max}$ is the maximum output power, Q is the load quality factor, f_{sw} is the switching frequency and f_{o} is the resonant frequency.

Let us consider the following parameters for the power inverter: $P_{\max} = 3500$ W, $Q \in [1, 8]$, $f_{\mathrm{sw}} \in [30$ kHz, 70 kHz], and $f_{\mathrm{o}} = 30$ kHz. The relative power resolution PR_{r} is defined as:

$$PR_{\mathrm{r}} = \max_{f_{\mathrm{sw}}, Q} \left\{ 100 \cdot \left| \frac{P(f_{\mathrm{sw}}) - P(f_{\mathrm{sw}} + \Delta f_{\mathrm{sw,min}})}{P(f_{\mathrm{sw}})} \right| \right\} \tag{4}$$

Assuming $f_{\mathrm{CLK}} = 25$ MHz, the minimum value of PA parameter N to fulfill a requirement of $PR_{\mathrm{r}} \leq 1$ % is $N = 21$ bits. With this parameters, the PAB-PWM frequency resolution is $\Delta f_{\mathrm{sw,min}} = 11.92$ Hz, and $PR_{\mathrm{r}} = 0.6$ %. With the same clock frequency, the CB-PWM achieves $PR_{\mathrm{r}} = 2.03\%$. The clock frequency has to be quadrupled to achieve the same relative power resolution than the PAB-PWM. These PA parameters ($f_{\mathrm{CLK}} = 25$ MHz, $N = 21$) will be used in the remainder of this paper.

B. Spectrum of the PAB-PWM output

The output spectrum of the square signa
CB-PWM with $D = 0.5$ only contains frequ
at $f_{\rm sw}$ and its odd integer multiples. Le
mechanism that makes that frequencies diffe
odd harmonics of $f_{\rm sw}$ appear in the output sp
signal generated by the PAB-PWM.

In a digital implementation, the switchin
an integer number of clock cycles; thus, wh
after division of 2^N by Δ is not zero, i.e. re
(1), two frequencies $f_{\rm swH}$ and $f_{\rm swL}$ are gen

$$f_{\rm swH} = \frac{f_{\rm CLK}}{\lfloor 2^N/\Delta \rfloor}$$
$$f_{\rm swL} = \frac{f_{\rm CLK}}{\lceil 2^N/\Delta \rceil}$$

Assuming $x \in \Re$, symbol $\lceil x \rceil$ represents
bigger than or equal to its real type argument x, and $\lfloor x \rfloor$
represents the greatest integer smaller than or equal to x.
According to the analysis presented in [30], the PA begins
to repeat its sequence after a number of clock cycles called
the Grand Repetition Rate (GRR):

$$GRR = \frac{2^N}{\gcd(2^N, \Delta)} \tag{6}$$

where gcd stands for greatest common divisor. The number of accumulator overflows, $N_{\rm OV}$, that occur in the phase accumulator over the period of GRR, i.e. the number of switching periods, is [30]:

$$N_{\rm OV} = \frac{\Delta}{\gcd(2^N, \Delta)} \tag{7}$$

The frequencies $f_{\rm swH}$ and $f_{\rm swL}$ are distributed over $N_{\rm OV}$ switching periods, such that the average switching frequency is given by (1). This can be seen as a switching frequency modulation effect, and sideband harmonics are expected to appear in the spectrum of the output signal [31]. Due to the GRR periodicity, the difference between two adjacent sideband harmonics is expected to be:

$$f_{\rm GRR} = \frac{f_{\rm CLK}}{GRR} \tag{8}$$

Let $PA_{\rm W}(j)$, and $f_{\rm sw}(j)$ be respectively the minimum PA value, and the generated frequency at switching period j. $PA_{\rm W}(j)$ is also the PA value after wraparound in the previous switching period. Assuming that $PA_{\rm W}(1) = 0$, the following conditions are met:

- $PA_{\rm W}(j)$ has period $N_{\rm OV}$, and $PA_{\rm W}(N_{\rm OV}+1)$ = 0.
- $PA_{\rm W}(j) < \Delta, \forall j, 1 \le j \le N_{\rm OV}$.
- $f_{\rm sw}(j) = f_{\rm swL}$ when $PA_{\rm W}(j) < {\rm rem}(2^N, \Delta)$, and $f_{\rm swH}$ otherwise.

Fig. 2 shows the PA sequence for $N = 4$ and $\Delta = 3$. Using the above equations, we have the following values: $\langle f_{\rm sw} \rangle = 3f_{\rm CLK}/16$, $f_{\rm swH} = f_{\rm CLK}/5$, $f_{\rm swL} = f_{\rm CLK}/6$, $f_{\rm GRR} = f_{\rm CLK}/16$, $N_{\rm OV} = 3$, $PA_{\rm W}(1) = 0$, $PA_{\rm W}(2) = 2$, $PA_{\rm W}(3) = 1$, $f_{\rm sw}(1) = f_{\rm swL}$, $f_{\rm sw}(2) = f_{\rm swH}$, $f_{\rm sw}(3) = f_{\rm swH}$. For duty cycle $D = 0.5$, the PAB-PWM output can be generated by complementing the PA most significant bit.

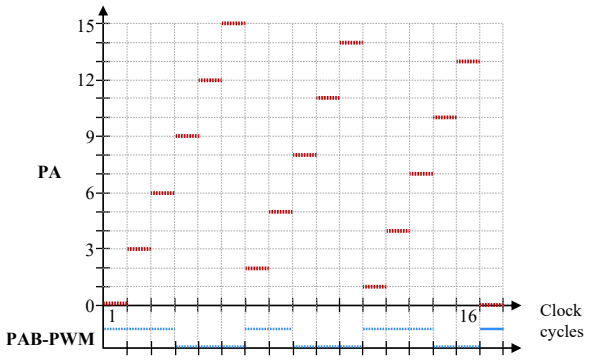

Fig. 2. Phase accumulator sequence for N=4 and Δ=3; and PAB-PWM output for D=0.5.

The values of $PA_{\rm W}(j)$ are distributed such that its average value is $\langle PA_{\rm W}(j) \rangle = {\rm rem}(2^N, \Delta)$. When $PA_{\rm W}(j)$ is plotted for $1 \le j \le N_{\rm OV}$, some sawtooth shaped patterns appear with higher frequency than $f_{\rm GRR}$. The $PA_{\rm W}(2)$ and $PA_{\rm W}(N_{\rm OV})$ values are given by:

$$\begin{aligned} PA_{\rm W}(2) &= \Delta - {\rm rem}(2^N, \Delta) \\ PA_{\rm W}(N_{\rm OV}) &= {\rm rem}(2^N, \Delta) \end{aligned} \tag{9}$$

The relationship between $PA_{\rm W}(2)$ and $PA_{\rm W}(N_{\rm OV})$ determines whether the sawtooth waveform ramps up or down. When $PA_{\rm W}(2) < PA_{\rm W}(N_{\rm OV})$, the ramp is upwards; otherwise it is downwards. Then, the sawtooth waveform ramps up or down at a rate of Ω:

$$\Omega = \min\left[{\rm rem}(2^N, \Delta), \Delta - rem(2^N, \Delta)\right] \tag{10}$$

Therefore, the sawtooth waveform has a frequency:

$$f_{\rm saw} \approx \frac{\langle f_{\rm sw} \rangle}{\Delta/\Omega} \tag{11}$$

In the example shown in Fig. 2, $PA_{\rm W}(2) > PA_{\rm W}(3)$, thus the plot of $PA_{\rm W}(j)$ for $1 \le j \le N_{\rm OV}$, is a sawtooth waveform that ramps down; $\Omega = 1$, and $f_{\rm saw} = f_{\rm GRR}$.

The pattern in $PA_{\rm W}(j)$ reflects onto the generated switching frequency since the generated switching frequency is $f_{\rm swL}$ or $f_{\rm swH}$ depending on $PA_{\rm W}(j)$ as explained above. Thus, when ${\rm rem}(2^N, \Delta) \neq 0$, the switching frequency is modulated in frequency with $f_{\rm m} = f_{\rm saw}$. The modulation profile is rectangular since only two frequencies are generated, and sidebands separated by the modulation frequency $f_{\rm m}$ are expected to appear on both sides of the switching frequency.

Fig. 3 shows these patterns for $N = 21$, $f_{\rm CLK} = 25$ MHz, and three Δ values. In cases (a), (c) and (d), $PA_{\rm W}(j)$ is represented over the whole range: $1 \le j \le N_{\rm OV}$. They all have a sawtooth shaped waveform but the period is very different from GRR. Fig. 3.(a) shows the values of $PA_{\rm W}$ for $\Delta = 4095$; using the above equations we have: $\langle f_{\rm sw} \rangle = 48816$ Hz, $N_{\rm OV} = 4095$, $f_{\rm m} = 6.1$ kHz, and $f_{\rm GRR} = 11.92$ Hz. Fig. 3.(b) shows a zoom-in of Fig. 3.(a) in order to appreciate the higher frequency patterns. Fig. 3.(c) shows the case for $\Delta = 4788$; thus: $\langle f_{\rm sw} \rangle = 57077$ Hz, $N_{\rm OV} = 1197$, $f_{\rm m} = 95.37$ Hz, and $f_{\rm GRR} = 47.68$ Hz. Fig. 3.(d) shows the

This article has been accepted for publication in a future issue of this journal, but has not been fully edited. Content may change prior to final publication. Citation information: DOI 10.1109/TIE.2018.2870351, IEEE Transactions on Industrial Electronics

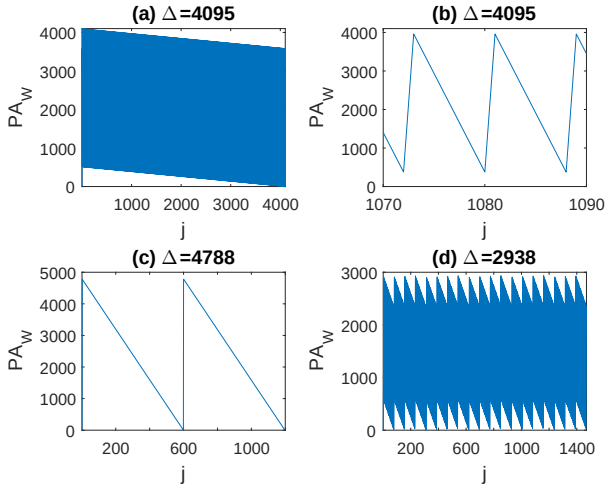

Fig. 3. PA_{W} in several cases: (a) Δ=4095, (b) zoom-in of Δ=4095, (c) Δ=4788, (d) Δ=2938, for the PAB-PWM parameters in section II.

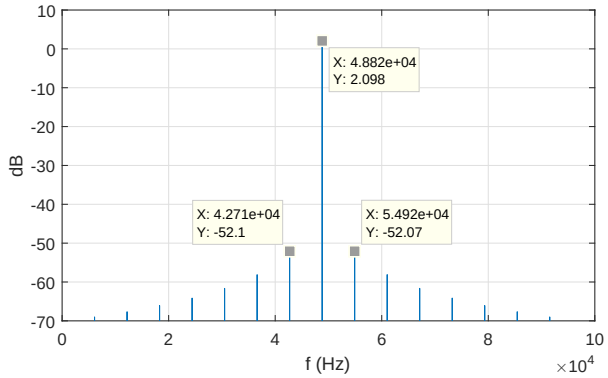

Fig. 4. Simulated spectrum of the PAB-PWM output with Δ=4095.

case of $\Delta = 2938$; thus: $\langle f_{\mathrm{sw}} \rangle = 35024$ Hz, $N_{\mathrm{OV}} = 1469$, $f_{\mathrm{m}} = 6.91$ kHz, and $f_{\mathrm{GRR}} = 23.84$ Hz. The pattern is more complex but the higher frequency is correctly calculated by (11). We have seen that the modulation frequency f_{m} can be much higher than the grand repetition rate frequency f_{GRR}.

Fig. 4 shows the simulated spectrum of the square wave generated by the PAB-PWM with $\Delta = 4095$ assuming that the output has values 1 and -1. The separation in frequency between adjacent sidebands corresponds exactly with the computed value of $f_{\mathrm{m}} = 6.1$ kHz.

C. Spur reduction technique

When DDS is used to generate a sine wave, several spur-reduction techniques are used in the literature to improve the Spurious Free Dynamic Range (SFDR). Two of these techniques are applied to the PAB-PWM modulator in this paper, and their effect on the audible noise is analyzed. These techniques are: the odd number and the phase dithering. The first one selects the Δ parameter to be an odd number. This technique maximizes the GRR and spreads out the spurs [11]. GRR is increased because when Δ is an odd number, then gcd$(2^N, \Delta)$ = 1 in (6), and GRR = 2^N.The second one is the phase dithering technique [28] that is applied when the generated signal is a square waveform. It consist in adding to the nominal value of Δ a random number in the interval $[-\Delta, \Delta]$ once every switching period. This technique breaks up the patterns in $PA_{\mathrm{W}}(j)$ while keeping the average switching frequency unchanged.

Notice that if the PA is reset after wraparound, i.e., $PA_{\mathrm{W}}(j) = 0\ \forall j$, then the generated switching frequency is f_{swL}, the constant frequency resolution is lost, and the relationship between the input parameter Δ and the output frequency becomes nonlinear since two input parameters can give the same output frequency.

D. Current harmonics effect on magnetic force

The source of acoustic noise is electromagnetic due to Lorentz forces exerted on the pot that can cause the pot to vibrate producing structure-borne acoustic noise. The magnetic flux density generated by the inductor exerts a force on the pot through the induced eddy currents on its bottom. The mechanical response to this forces can generate acoustic noise. The magnetic force is proportional to the inductor current squared as shown by simulation in [25]. This force can be calculated by integrating the Lorentz force density $\boldsymbol{J} \times \boldsymbol{B}$. The induced eddy current density $\boldsymbol{J}$ has only azimuthal component (J_θ), and the magnetic flux density $\boldsymbol{B}$ has radial and vertical components (B_r, B_z) due to the cylindrical symmetry [32]. The cross product has radial and vertical components:

$$\boldsymbol{J} \times \boldsymbol{B} = \begin{vmatrix} \hat{\boldsymbol{r}} & \hat{\boldsymbol{\theta}} & \hat{\boldsymbol{z}} \\ 0 & J_\theta & 0 \\ B_r & 0 & B_z \end{vmatrix} = J_\theta \cdot B_z \hat{\boldsymbol{r}} - J_\theta \cdot B_r \hat{\boldsymbol{z}} \qquad (12)$$

Assuming that the inductor carries a sinusoidal current, and the pot material is linear, the magnetic flux density and the induced current density are proportional to the current amplitude [32]. Thus, the radial and vertical forces are proportional to the inductor current squared.

In the case of PAB-PWM, when rem$(2^N, \Delta) \neq 0$, the sideband harmonics that appear in the spectrum of the output signal (the output voltage of the half bridge inverter) will also appear in the inductor current spectrum. Thus, the inductor current can be expressed as the sum of sinusoidal signals with frequencies $f_{n,h} = nf_{\mathrm{sw}} \pm hf_{\mathrm{m}}$. Applying the windowing theorem [26], the harmonics of i_{L}^2 can be obtained from the harmonics of i_{L}. The components in i_{L}^2 with frequencies $(f_{n,h} + f_{n',h'})$ will lie outside the audible range since f_{sw} is above 20 kHz. Only, the components in i_{L}^2 with frequencies $(f_{n,h} - f_{n',h'})$ such that $n = n'$ will produce magnetic forces with frequencies that are integer multiples of f_{m} and can lie inside the range 5 kHz - 20 kHz. In the case of CB-PWM, no sidebands appear, $h = h' = 0$, and all the frequencies lie outside the above audible range.

Additionally, due to the amplitude modulation of the bus voltage in Fig. 1, the inductor current also has components at frequencies $nf_{\mathrm{sw}} \pm hf_{\mathrm{B}}$ [33], where $f_{\mathrm{B}} = 100$ Hz (double of the mains frequency). The difference between current harmonics of the same harmonic number n will produce low frequency bass tones that lie outside the range 5 kHz - 20 kHz that we have set above. They are not taken into account in the remainder of the paper because they cannot be avoided.

This article has been accepted for publication in a future issue of this journal, but has not been fully edited. Content may change prior to final publication. Citation information: DOI 10.1109/TIE.2018.2870351, IEEE Transactions on Industrial Electronics

III. Simulation Results

The coupled electromagnetic, structural and acoustic simulation of the system is out of the scope of this work. Since the electromagnetic force (proportional to the inductor current squared), and the emitted acoustic noise are expected to have the same frequency components in their spectra, only the spectral analysis of the load current will be carried out in this section. Thus, the circuit of Fig. 1 (without the EMI filter and snubber capacitors) is simulated using Matlab/Simulink. The circuit parameters are $C = 1080$ nF, $L = 30$ μH, and $R = 3\ \Omega$. The bus voltage is an ideal full-wave rectified sinusoid with period $T_{\rm B} = 10$ ms, and amplitude 325 V. The PAB-PWM with and without phase dithering, and CB-PWM modulations are simulated.

The value of the inductor current is recorded during $T_{\rm B}$, and the DFT (Discrete Fourier Transform) is applied to get the simulated spectrum of $i_{\rm L}^2$. The DFT frequency resolution is 100 Hz. The sampling frequency $f_{\rm s}$ is equal to the clock frequency.

SFM (Spectral Flatness Measure) [27] will be used to quantify the noise-like or tone-like nature of the spectrum of $i_{\rm L}^2$ in the band [5 kHz - 20 kHz]. SFM is computed as the ratio of the geometric mean and the arithmetic mean of the $i_{\rm L}^2$ spectrum:

$$SFM = \frac{\left(\prod_{k=K_1}^{K_2} i_{\rm L}^2[k]\right)^{\frac{1}{K_2-K_1+1}}}{\frac{1}{K_2-K_1+1}\sum_{k=K_1}^{K2} i_{\rm L}^2[k]} \tag{13}$$

where $i_{\rm L}^2[k]$ is the magnitude of the k-th DFT coefficient. For an N-point DFT, $i_{\rm L}^2[k]$ corresponds to the frequency $(k/N)\cdot f_{\rm s}$ Hz. Thus, the limits K_1 and K_2 are the DFT k-th indexes corresponding to 5 kHz and 20 kHz respectively. For tonal signals, SFM is close to 0; and it is close to 1 for noise signals.

Fig. 5.(a) shows the simulated spectrum of the inductor current generated by the inverter operated with PAB-PWM and $\Delta = 4095$ ($\langle f_{\rm sw}\rangle = 48816$ Hz). Several sidebands appear on both sides of the switching frequency. The 6.1 kHz frequency difference between the sidebands, theoretically predicted in last section, will generate tones at multiples of this frequency in $i_{\rm L}^2$. Fig. 5.(b) shows the spectrum of $i_{\rm L}^2$ where we can see three tones at multiples of 6.1 kHz in the acoustic frequency range of interest. These frequencies will also appear in the acoustic noise spectrum as we will show in the experimental results. The magnitude of the acoustic noise at each component will depend on the pot. Moreover, SFM is close to zero (0.0036), indicating the tonal nature of $i_{\rm L}^2$ in this frequency band.

Fig. 6 shows the simulated spectrum of the inductor current generated by the inverter operated with PAB-PWM and $\Delta = 4788$ ($\langle f_{\rm sw}\rangle = 57077$ Hz). SFM is close to one (0.9223). In the spectrum of the inductor current, no sideband harmonics appear, thus, no pure tones will appear in the spectrum of $i_{\rm L}^2$ above 5 kHz, and no tones will appear in the range where noise may be audible, as it will be shown in next section.

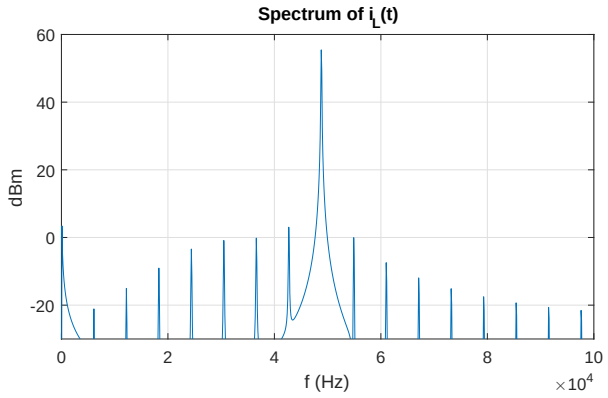

(a)

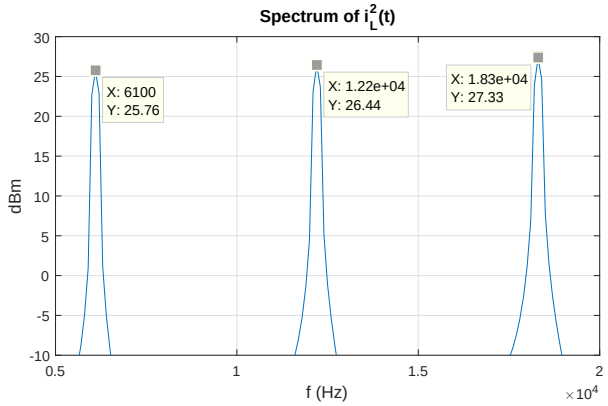

(b)

Fig. 5. Simulated spectrum of PAB-PWM with Δ=4095. (a) $i_{\rm L}$, (b) $i_{\rm L}^2$

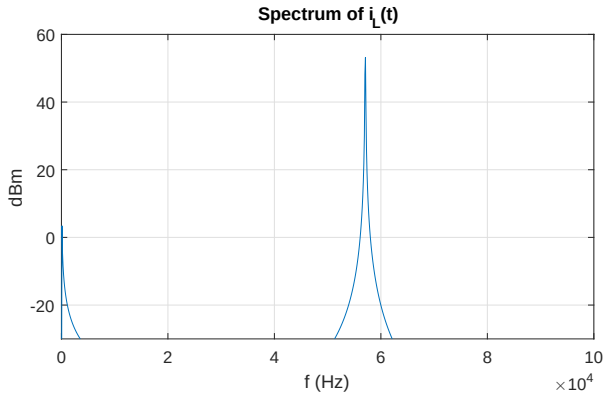

Fig. 6. Spectrum of $i_{\rm L}$ with PAB-PWM and Δ=4788.

Fig. 7 shows the simulated normalized distribution of SFM values for switching frequencies between 30 kHz and 70 kHz selecting Δ parameter to be an odd number. Many cases with low values of SFM appear when Δ is an odd number, then the example above with $\Delta = 4095$ (odd number) was not an isolated case. Thus, this technique reported in the literature [11] is not adequate to reduce the acoustic noise in this application.

Next, the phase dithering technique presented in [28] is going to be tested in this application. The PAB-PWM without and with the phase dithering technique enabled is compared with the CB-PWM since it is known that the latter does not

This article has been accepted for publication in a future issue of this journal, but has not been fully edited. Content may change prior to final publication. Citation information: DOI 10.1109/TIE.2018.2870351, IEEE Transactions on Industrial Electronics

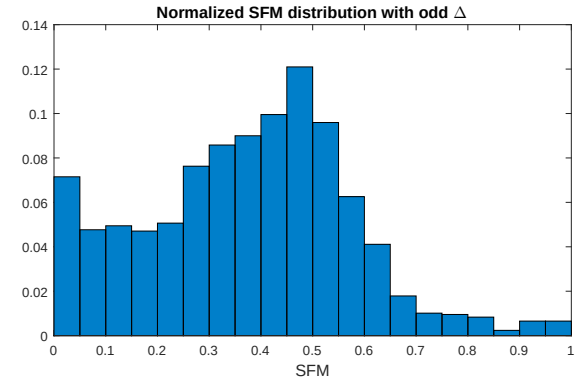

Fig. 7. SFM normalized distribution with odd Δ values.

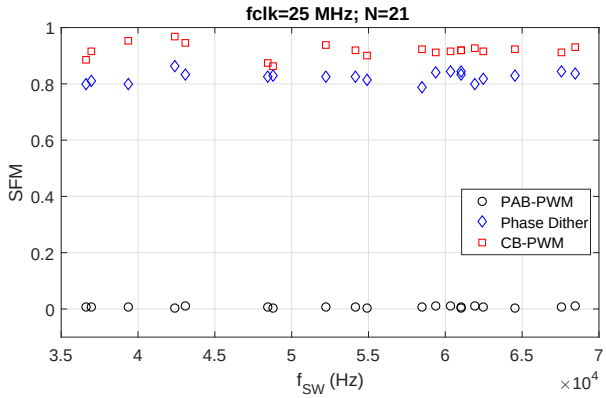

Fig. 8. Comparison between modulation strategies of SFM values for several switching frequencies. Modulator parameters: f_{CLK}=25 MHz, N=21.

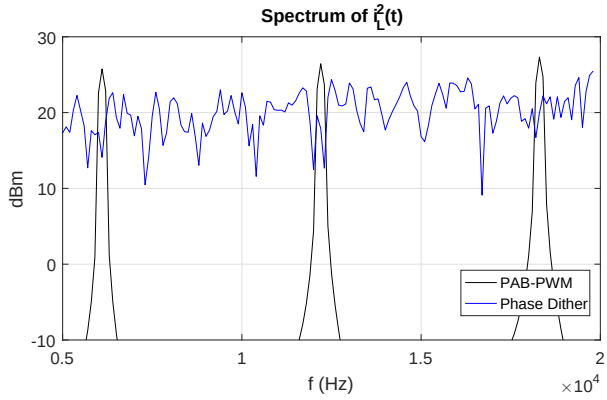

Fig. 9. Spectrum of i_{L}^2 under PAB-PWM control strategy with Δ=4095, without and with phase dithering enabled.

generate acoustic noise. The N_{C} parameter in the CB-PWM is chosen to be $N_{\mathrm{C}} = \lceil 2^N/\Delta \rceil$, then, the CB-PWM generates switching frequency f_{swL}.

Fig. 8 shows the simulated SFM values for 20 switching frequencies with the lowest SFM values. SFM increases when the phase dithering technique is enabled in the PAB-PWM. The biggest SFM values are obtained with the CB-PWM as expected. These values are taken as an upper limit for the other technique.

Fig. 9 compares the simulated spectrum of i_{L}^2 under PAB-PWM control with $\Delta = 4095$ when the phase dithering technique is disabled and enabled. Pure tones are suppressed in the spectrum of i_{L}^2 when it is enabled, but at the expense of increasing the noise floor. Thus, it is expected to be noisy [15], although less annoying to the user than without dithering because of suppression of pure tones.

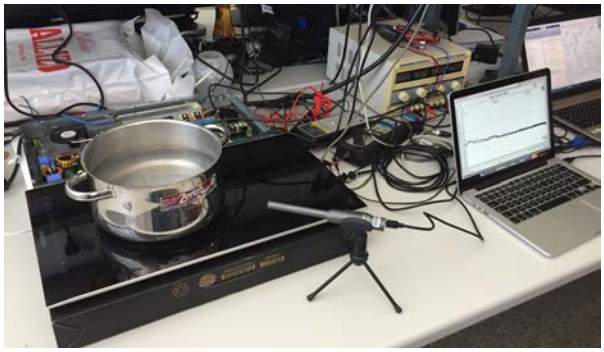

Fig. 10. Experimental setup for the acoustic noise measurement.

TABLE I
CIRCUIT PARAMETERS OF THE PROTOTYPE

Symbol	Description	Value
$\hat{V}_{\mathrm{B}}$	Peak bus voltage	325 V
f_{grid}	Line frequency	50 Hz
R	Load equivalent resistance	3.2 Ω
L	Load equivalent inductance	28 μF
C_{B}	Bus capacitor	3.3 μF
C_{r}	Resonance capacitor	1080 nF
C_{s}	Snubber capacitor	15 nF

IV. EXPERIMENTAL RESULTS

Fig. 10 shows the experimental setup. It consists of a resonant half-bridge inverter that is fed by the rectified mains. The resonant inverter is loaded with a planar spiral inductor with an external diameter of 21 cm, and a commercial pot filled with water is placed above the inductor. The inverter and induction load parameters are summarized in Table I.

The PAB-PWM and CB-PWM are implemented in an FPGA (Field Programmable Gate Array) Zynq 7020 of Xilinx. Linear feedback shift registers (LFSR) are used to generate pseudo random binary sequences [34], and they can be efficiently implemented in FPGAs. The feedback coefficients are expressed as a polynomial and if the polynomial is primitive, the LFSR generates a maximum length sequence. This primitive polynomials are listed in many books and articles [34]. The random numbers for the phase dithering technique are generated using an 18-bit LFSR whose characteristic polynomial is $P(x) = x^{18} + x^7 + 1$. A new random number is generated once every switching period.

The acoustic noise is measured with a calibrated MiniDSP UMIK-1 measurement microphone. It features low noise and accurate results ($\pm$1 dB) over the 20 Hz to 20 kHz range. The inductor current during T_{B} has been measured and digitized with an oscilloscope Tektronix MDO 3014 at a sampling

This article has been accepted for publication in a future issue of this journal, but has not been fully edited. Content may change prior to final publication. Citation information: DOI 10.1109/TIE.2018.2870351, IEEE Transactions on Industrial Electronics

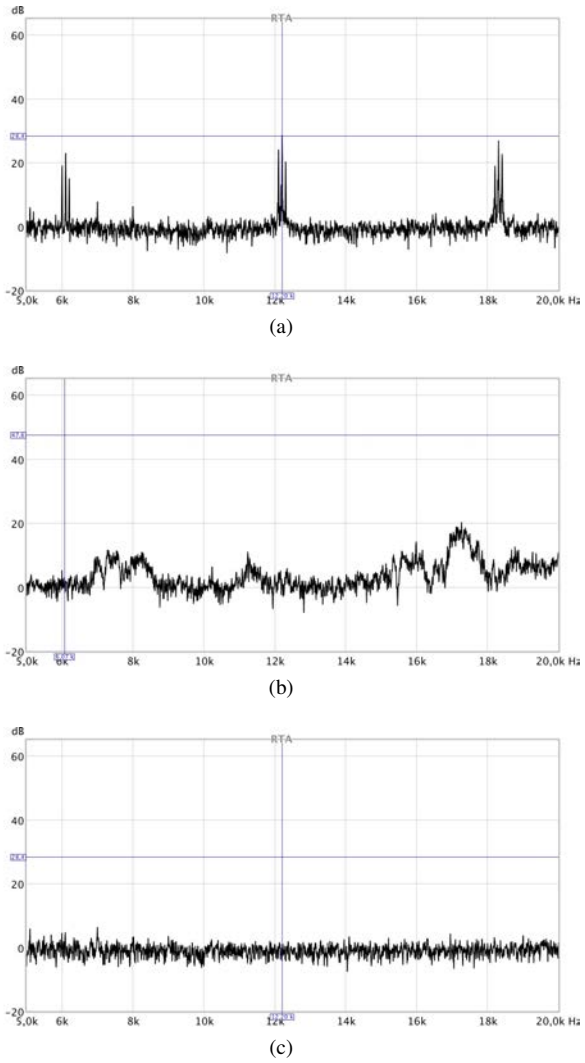

Fig. 11. Measured acoustic noise spectra for different modulation strategies with Δ=4095: (a) PAB-PWM, (b) PAM-PWM with phase dithering enabled, (c) CB-PWM.

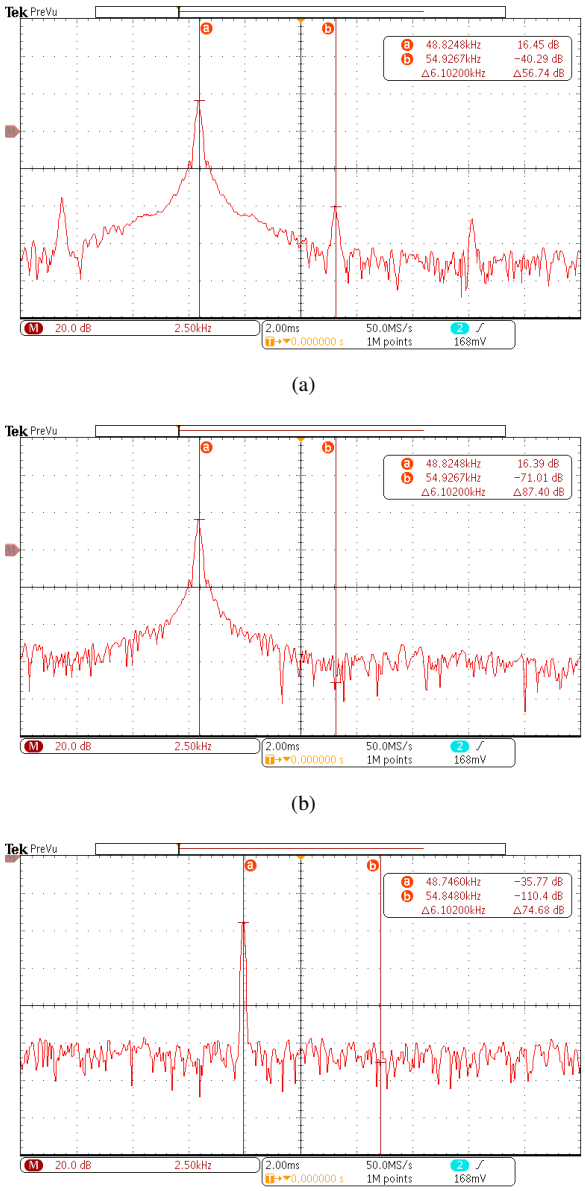

Fig. 12. Measured inductor current spectra for different modulation strategies with Δ=4095: (a) PAB-PWM, (b) PAB-PWM with phase dithering enabled, (c) CB-PWM.

frequency of 50 Msps. The fan is switched off and measures are taken before the boiling phase in order to reduce additional noise sources. The audible noise spectrum and the electric spectrum of the inductor current are measured to test the correlation between them.

Fig. 11 shows the measured acoustic noise spectra generated with $\Delta = 4095$ in three cases. Fig. 11.(a) shows the spectrum with the PAB-PWM. Large tones appear in the audible noise spectrum at multiples of 6.1 kHz as calculated theoretically. Fig. 11.(b) shows the spectrum with the phase dithering technique enabled; pure tones have been eliminated but the emitted sound is louder and it is perceived as unpleasant. Fig. 11.(c) shows the spectrum when the CB-PWM is applied. This last measurement is the reference to compare with since, as it is known, it does not generate acoustic noise.

Fig. 12.(a) shows the measured spectrum of the inductor current in the PAB-PWM case. It can be seen the biggest harmonic at the switching frequency (cursor a) and that the distance between sidebands corresponds with the frequencies of the tones in the acoustic noise spectrum. Fig. 12.(b) shows the measured current spectrum when the phase dithering technique is applied. There are not sidebands, but the noise floor is higher than in case (a). Fig. 12.(c) shows the spectrum in the CB-PWM case.

Fig. 13 shows the measured acoustic noise spectra generated with PAB-PWM with $\Delta = 4788$. Tones does not appear in the audible noise spectrum as calculated theoretically; SFM is close to one (0.9223).

Fig. 14 and Fig. 15 show experimental waveforms at two different power conditions, low and high, respectively. Three modulation schemes (PAB-PWM, PAB-PWM with phase dithering, and CB-PWM) are shown for each power condition. Each figure shows the following waveforms: the input voltage, the output voltage, the input current, and the load current. Zooms of these waveforms during a few switching cycles are

This article has been accepted for publication in a future issue of this journal, but has not been fully edited. Content may change prior to final publication. Citation information: DOI 10.1109/TIE.2018.2870351, IEEE Transactions on Industrial Electronics

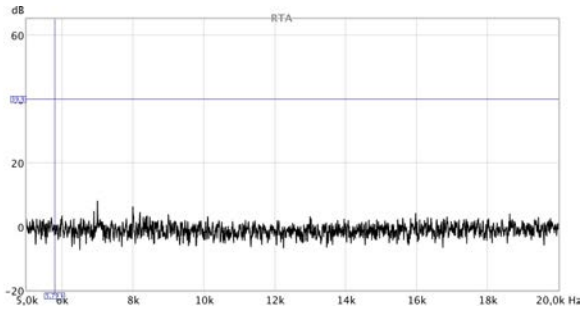

Fig. 13. Measured acoustic noise spectrum for PAB-PWM with phase dithering disabled and Δ=4788.

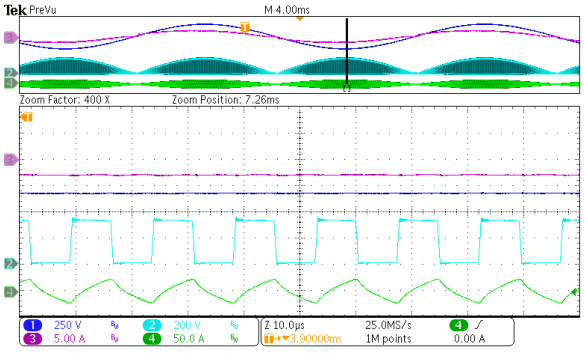

(a)

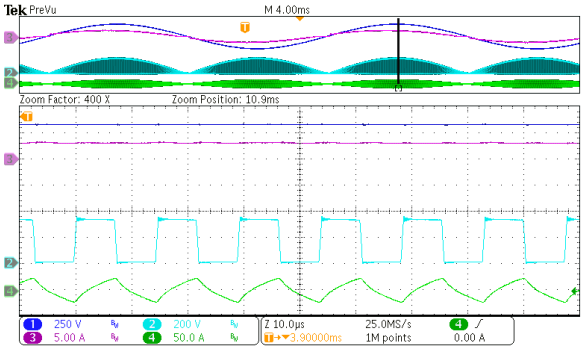

(b)

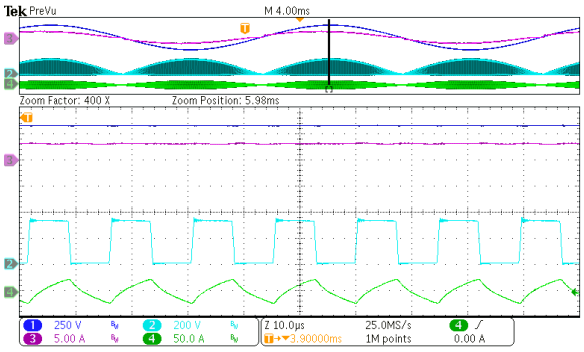

(c)

Fig. 14. Experimental waveforms for different modulation strategies with Δ = 5743. Input voltage (Ch1: 250 V/div), output voltage (Ch2: 200 V/div), input current (Ch3: 5 A/div) and load current (Ch4: 50 A/div). (a) PAB-PWM, (b) PAB-PWM with phase dithering enabled, (c) CB-PWM.

shown at around the maximum value of the input voltage. The waveforms shown in these pictures were captured without EMI

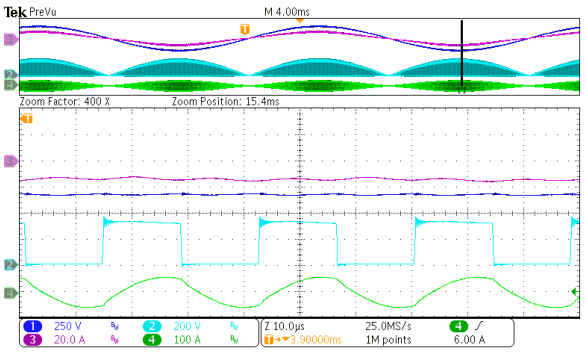

(a)

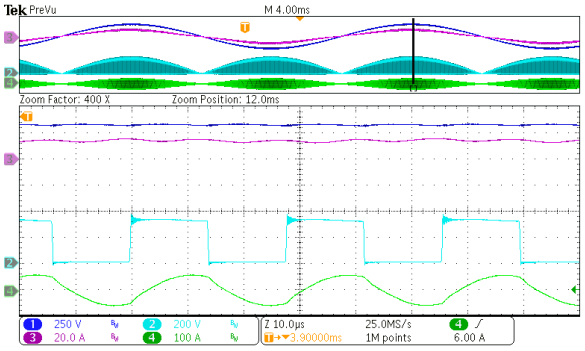

(b)

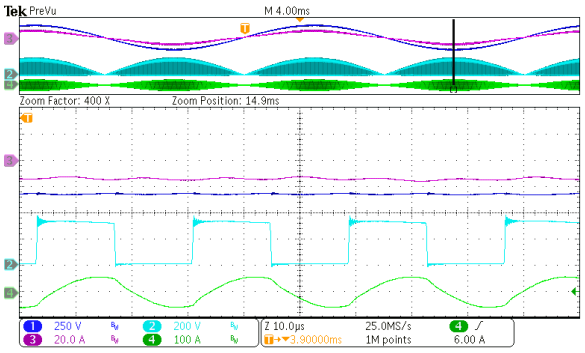

(c)

Fig. 15. Experimental waveforms for different modulation strategies with Δ = 3011. Input voltage (Ch1: 250 V/div), output voltage (Ch2: 200 V/div), input current (Ch3: 20 A/div) and load current (Ch4: 100 A/div). (a) PAB-PWM, (b) PAB-PWM with phase dithering enabled, (c) CB-PWM.

filter and with the converter fed by a Chroma AC source model 61605. The acoustic noise measurements were taken with the converter fed by the mains in order to avoid the acoustic noise generated by the Chroma AC source.

Fig. 14 shows the main converter waveforms with Δ = 5743 and the three modulation strategies. Fig. 14.(a) shows the experimental waveforms with the PAB-PWM. Fig. 14.(b) shows the waveforms with the PAB-PWM and phase dithering enabled. Fig. 14.(c) shows the waveforms with the CB-PWM. In all three cases, f_{sw} is around 68 kHz, the power delivered by the AC source (P_{i}) is 500 W, and the Power Factor (PF) is 0.976. The values of P_{i}, and PF have been measured by the Chroma AC source. Input current distortion due to rectifier and bus capacitor filter C_{B} can be appreciated in the zero crossings of the mains voltage. Thus, it can be observed that given a

Δ parameter (that determines the switching frequency), the input current waveforms are similar for the three modulation schemes, but not its results regarding acoustic noise.

Fig. 15 shows the main converter waveforms with $\Delta = 3011$ and the three modulation strategies. Fig. 15.(a) shows the waveforms with the PAB-PWM. Fig. 15.(b) shows the waveforms with the PAB-PWM and phase dithering enabled. Fig. 15.(c) shows the waveforms with the CB-PWM. In all three cases, f_{sw} is around 36 kHz, P_{i} is 2129 W, and PF is 0.994.

The relationship between the frequencies that appear in the acoustic noise spectrum and the distance between sidebands in the spectrum of the inductor current has been experimentally verified when the inverter is operated under PAB-PWM. As expected, the phase dithering technique reduces the tones at the expense of increasing the noise floor what can be annoying for the user.

V. Conclusion

This paper compares the well-established CB-PWM with the PAB-PWM from the acoustic point of view in a domestic IH application.

1) The PAB-PWM technique can produce annoying acoustic tones when $\mathrm{rem}(2^N, \Delta) \neq 0$ because the switching frequency is modulated in frequency. The modulation profile is rectangular since only two frequencies are generated.
2) The theoretical analysis of the frequency components generated by the PAB-PWM yields to an equation, (11), that allows to predict the highest modulation frequency f_{m} from the phase accumulator parameters and then the frequencies of the generated acoustic tones. The frequency of these tones can be much higher than the grand repetition rate frequency f_{GRR}.
3) The spectral flatness measure (SFM) of i_{L}^2 in the frequency range of interest, has revealed to be a good merit figure to detect at which frequencies PAB-PWM generates acoustic noise.
4) It has been shown that the technique of selecting Δ an odd number, that is reported in the DDS literature as a spur reduction technique, is not adequate to reduce the acoustic noise in this application.
5) Although the PAB-PWM modulation technique has several advantages over the CB-PWM, the latter outperforms the acoustic behavior of the former. In order to use the PAB-PWM in domestic IH applications, other noise reduction techniques should be investigated since increasing the audible noise emissions of an appliance is not a satisfactory result for manufacturers.

All theoretical results have been experimentally verified by acoustic noise measurements in a domestic IH prototype.

References

[1] O. Lucia, J. M. Burdio, I. Millan, J. Acero, and D. Puyal, "Load-adaptive control algorithm of half-bridge series resonant inverter for domestic induction heating," *IEEE Transactions on Industrial Electronics*, vol. 56, DOI 10.1109/TIE.2009.2022516, no. 8, pp. 3106–3116, Aug. 2009.

[2] H. W. Koertzen, J. D. van Wyk, and J. A. Ferreira, "Design of the half-bridge, series resonant converter for induction cooking," in *Power Electronics Specialists Conference, 1995. PESC '95 Record., 26th Annual IEEE*, vol. 2, DOI 10.1109/PESC.1995.474899, pp. 729–735 vol.2, Jun. 1995.

[3] J. Acero, J. M. Burdio, L. A. Barragan, D. Navarro, R. Alonso, J. Ramon, F. Monterde, P. Hernandez, S. Llorente, and I. Garde, "Domestic induction appliances," *IEEE Industry Applications Magazine*, vol. 16, DOI 10.1109/MIAS.2009.935495, no. 2, pp. 39–47, Mar. 2010.

[4] H. Meuth, I. Janiszewski, and K. Schade, "Phase-accumulator based multi-channel high-precision digital PWM architecture," in *Proceedings of the 2005 IEEE International Frequency Control Symposium and Exposition, 2005.*, DOI 10.1109/FREQ.2005.1574011, pp. 646–651, Aug. 2005.

[5] O. Jimenez, O. Lucia, I. Urriza, L. A. Barragan, P. Mattavelli, and D. Boroyevich, "An FPGA-based gain-scheduled controller for resonant converters applied to induction cooktops," *IEEE Transactions on Power Electronics*, vol. 29, DOI 10.1109/TPEL.2013.2276041, no. 4, pp. 2143–2152, Apr. 2014.

[6] A. Dominguez, L. A. Barragan, A. Otin, D. Navarro, and D. Puyal, "Inverse-based power control in domestic induction-heating applications," *IEEE Transactions on Industrial Electronics*, vol. 61, DOI 10.1109/TIE.2013.2281155, no. 5, pp. 2612–2621, May. 2014.

[7] L. A. Barragan, D. Navarro, J. Acero, I. Urriza, and J. M. Burdio, "FPGA implementation of a switching frequency modulation circuit for emi reduction in resonant inverters for induction heating appliances," *IEEE Transactions on Industrial Electronics*, vol. 55, DOI 10.1109/TIE.2007.896129, no. 1, pp. 11–20, Jan. 2008.

[8] C. Carretero, O. Lucia, J. Acero, and J. M. Burdio, "Phase-shift modulation in double half-bridge inverter with common resonant capacitor for induction heating appliances," *IET Power Electronics*, vol. 8, DOI 10.1049/iet-pel.2014.0229, no. 7, pp. 1128–1136, 2015.

[9] M. Tahir, G. R. Walker, M. A. H. Broadmeadow, S. M. Bulmer, and G. F. Ledwich, "Comparative analysis of FPGA-based digital pulse width modulation techniques for multiphase dc-dc converters," in *2016 IEEE 2nd Annual Southern Power Electronics Conference (SPEC)*, DOI 10.1109/SPEC.2016.7846119, pp. 1–6, Dec. 2016.

[10] L. Cordesses, "Direct digital synthesis: a tool for periodic wave generation (part 1)," *IEEE Signal Processing Magazine*, vol. 21, DOI 10.1109/MSP.2004.1311140, no. 4, pp. 50–54, Jul. 2004.

[11] L. Cordesses, "Direct digital synthesis: a tool for periodic wave generation (part 2)," *IEEE Signal Processing Magazine*, vol. 21, DOI 10.1109/MSP.2004.1328096, no. 5, pp. 110–112, Sep. 2004.

[12] W. C. Lo, C. C. Chan, Z. Q. Zhu, L. Xu, D. Howe, and K. T. Chau, "Acoustic noise radiated by PWM-controlled induction machine drives," *IEEE Transactions on Industrial Electronics*, vol. 47, DOI 10.1109/41.857968, no. 4, pp. 880–889, Aug. 2000.

[13] M. M. Bech, J. K. Pedersen, and F. Blaabjerg, "Field-oriented control of an induction motor using random pulsewidth modulation," *IEEE Transactions on Industry Applications*, vol. 37, DOI 10.1109/28.968191, no. 6, pp. 1777–1785, Nov. 2001.

[14] A. Ruiz-Gonzalez, F. Vargas-Merino, J. R. Heredia-Larrubia, M. J. Meco-Gutierrez, and F. Perez-Hidalgo, "Application of slope PWM strategies to reduce acoustic noise radiated by inverter-fed induction motors," *IEEE Transactions on Industrial Electronics*, vol. 60, DOI 10.1109/TIE.2012.2196892, no. 7, pp. 2555–2563, Jul. 2013.

[15] I. P. Tsoumas and H. Tischmacher, "Influence of the inverter's modulation technique on the audible noise of electric motors," *IEEE Transactions on Industry Applications*, vol. 50, DOI 10.1109/TIA.2013.2268453, no. 1, pp. 269–278, Jan. 2014.

[16] A. C. Binojkumar, B. Saritha, and G. Narayanan, "Acoustic noise characterization of space-vector modulated induction motor drives - an experimental approach," *IEEE Transactions on Industrial Electronics*, vol. 62, DOI 10.1109/TIE.2014.2374557, no. 6, pp. 3362–3371, Jun. 2015.

[17] A. C. Binojkumar, B. Saritha, and G. Narayanan, "Experimental comparison of conventional and bus-clamping PWM methods based on electrical and acoustic noise spectra of induction motor drives," *IEEE Transactions on Industry Applications*, vol. 52, DOI 10.1109/TIA.2016.2584578, no. 5, pp. 4061–4073, Sep. 2016.

[18] O. Lucia, P. Maussion, E. J. Dede, and J. M. Burdio, "Induction heating technology and its applications: Past developments, current technology, and future challenges," *IEEE Transactions on Industrial Electronics*, vol. 61, DOI 10.1109/TIE.2013.2281162, no. 5, pp. 2509–2520, May. 2014.

[19] P. M. Gaudo, C. Bernal, J. Avellaned, and J. M. Burdio, "Intermodulation distortion in 1SW-ZVS multi-inverter for induction heating home appliances," in *2012 Twenty-Seventh Annual IEEE Applied Power Electronics Conference and Exposition (APEC)*, DOI 10.1109/APEC.2012.6166131, pp. 2223–2228, Feb. 2012.

[20] T. Haag, J. Bogel, and H. Friedrich, "Method and arrangement for supplying power to several induction coils in an induction apparatus," Patent U.S. 7 910 865 B2, Mar. 22, 2011.
[21] J. M. Burdio, L. A. Barragan, P. Hernandez, A. Lorente, F. Monterde, and S. Llorente, "Method for avoiding or reducing noise interference in a converter circuit with multiple simultaneously operated outputs," Patent EP1 683 257 (B1), 2011.
[22] C.-H. Cho and Y.-Y. Chen, "Heating device capable of eliminating noise and adjusting desired heat quality or heating temperature by controlling frequency difference between two induction coils during a first time interval and disabling one of two induction coils during a second interval," Patent U.S. 8 658 950 B2, Feb. 25, 2014.
[23] B. Sanchez, J. Llado, J. Ortiz, D. Valladares, C. Pina, S. Llorente, and P. Hernandez, "Acoustic characterization of an induction cooker," in *International Congress on Sound and Vibration*, pp. 156–162, 2006.
[24] H. Yonemori, M. Kobayashi, and K. Suzuki, "Temperature control of a double-coil drive type ih cooker by means of the PDM control provided with audio noise suppression," in *2008 15th IEEE International Conference on Electronics, Circuits and Systems*, DOI 10.1109/ICECS.2008.4675003, pp. 914–917, Aug. 2008.
[25] C. M. Zingerli, T. Nussbaumer, and J. W. Kolar, "Optimizing repulsive lorentz forces for a levitating induction cooker," in *2014 International Power Electronics Conference (IPEC-Hiroshima 2014 - ECCE ASIA)*, DOI 10.1109/IPEC.2014.6870170, pp. 3365–3370, May. 2014.
[26] J. G. Proakis and D. Manolakis, *Digital Signal Processing: principles, algorithms and applications*, 3rd ed. Prencite Hall, 1996.
[27] J. D. Johnston, "Transform coding of audio signals using perceptual noise criteria," *IEEE Journal on Selected Areas in Communications*, vol. 6, DOI 10.1109/49.608, no. 2, pp. 314–323, Feb. 1988.
[28] C. E. Wheatley and D. E. Phillips, "Spurious suppression in direct digital synthesizers," in *Thirty Fifth Annual Frequency Control Symposium*, DOI 10.1109/FREQ.1981.200508, pp. 428–435, May. 1981.
[29] J. M. Burdio, L. A. Barragan, F. Monterde, D. Navarro, and J. Acero, "Asymmetrical voltage-cancellation control for full-bridge series resonant inverters," *IEEE Transactions on Power Electronics*, vol. 19, DOI 10.1109/TPEL.2003.823250, no. 2, pp. 461–469, Mar. 2004.
[30] A technical tutorial on digital signal synthesis, Tech. Rep., Analog Devices Inc., 1999.
[31] S. Johnson and R. Zane, "Custom spectral shaping for emi reduction in high-frequency inverters and ballasts," *IEEE Transactions on Power Electronics*, vol. 20, DOI 10.1109/TPEL.2005.857565, no. 6, pp. 1499–1505, Nov. 2005.
[32] J. Acero, R. Alonso, L. A. Barragan, and J. M. Burdio, "Modeling of planar spiral inductors between two multilayer media for induction heating applications," *IEEE Transactions on Magnetics*, vol. 42, DOI 10.1109/TMAG.2006.882308, no. 11, pp. 3719–3729, Nov. 2006.
[33] O. Jimenez, O. Lucia, I. Urriza, L. A. Barragan, and D. Navarro, "Power measurement for resonant power converters applied to induction heating applications," *IEEE Transactions on Power Electronics*, vol. 29, DOI 10.1109/TPEL.2014.2304675, no. 12, pp. 6779–6788, Dec. 2014.
[34] R. N. Mutagi, "Pseudo noise sequences for engineers," *Electronics Communication Engineering Journal*, vol. 8, DOI 10.1049/ecej:19960205, no. 2, pp. 79–87, Apr. 1996.

Jorge Villa (S'18) received M.Sc. degree in industrial engineering from the University of Zaragoza, Zaragoza, Spain, in 2016, where he is currently working toward the Ph.D. degree in electronic engineering.

His main research interests include resonant converters and digital control for induction heating applications.

Mr. Villa is a member of the Aragon Institute for Engineering Research (I3A), Group of Power Electronics and Microelectronics (GEPM).

José I. Artigas received the M.Sc. and Ph.D. degrees in electrical engineering from the University of Zaragoza, Zaragoza, Spain, in 1989 and 1996, respectively.

He has been with the Department of Electronic Engineering and Communications, University of Zaragoza, where he is currently an Associate Professor. He has been involved in different research and development projects. His main research interests include signal acquisition, digital control, and modulation strategies applied to power converters.

Dr. Artigas is a member of the Aragón Institute for Engineering Research (I3A), Group of Power Electronics and Microelectronics (GEPM).

José R. Beltrán received the M.Sc. and Ph.D. degrees in Physics from the University of Zaragoza, Zaragoza, Spain, in 1988 and 1994, respectively.

He is an Associate Professor with the Department of Electronic Engineering and Communications, University of Zaragoza. He has been involved in different research and development projects on Audio Analysis and Processing. His research interests are focused on the study of Automatic Learning Systems for the analysis, processing and synthesis of the musical signal. In 2008, he was a promoter and founder of an academic spin-off: ARSTIC Audiovisual Solutions S.L. devoted to the use of technologies for the artistic and audiovisual fields.

Dr. Beltrán is a member of the Aragon Institute for Engineering Research (I3A), Research Group in Advanced Interfaces (AffectiveLab).

Alberto Domínguez received the Ph.D Degree in electronic engineering from the University of Zaragoza, Spain in 2017.

Since 2017, he is working by BSH Home Appliances in the development of new domestic induction cooktops. His main research interests include modeling, control and optimization of constrained systems, especially devoted to resonant inverters in domestic induction heating.

Luis A. Barragán received the M.Sc. and Ph.D. degrees in physics from the University of Zaragoza, Zaragoza, Spain, in 1988 and 1993, respectively.

He is an Associate Professor with the Department of Electronic Engineering and Communications, University of Zaragoza. He has been involved in different research and development projects on induction-heating systems for home appliances. His research interests include modeling and digital control applied to domestic induction heating.

Dr. Barragán is a member of the Aragon Institute for Engineering Research (I3A), Group of Power Electronics and Microelectronics (GEPM).